Characterization of the Platinum–Hydrogen Bond by Surface-Sensitive Time-Resolved Infrared Spectroscopy

Paleček, David ; Tek, Gökçen ; Lan, Jinggang ; Iannuzzi, Marcella ; Hamm, Peter

DOI: https://doi.org/10.1021/acs.jpclett.8b00310

Characterization of the Platinum-Hydrogen Bond by Surface-Sensitive Time-Resolved Infrared Spectroscopy

David Paleček, Gökçen Tek, Jinggang Lan, Marcella Iannuzzi, and Peter Hamm

Department of Chemistry, University of Zurich, Zurich, Switzerland

corresponding author: peter.hamm@chem.uzh.ch

(Dated: February 23, 2018)

Abstract

Abstract: The vibrational dynamics of Pt-H on a nano-structured platinum surface has been examined by ultrafast infrared spectroscopy. Three bands are observed at 1800 cm^{-1}, 2000 cm^{-1} and 2090 cm^{-1}, which are assigned to Pt-CO in a bridged and linear configuration, as well as Pt-H, respectively. Lifetime analysis revealed a time constant of (0.8 ± 0.1) ps for the Pt-H mode, considerably shorter than that of Pt-CO due to its stronger coupling to the metal substrate. 2D attenuated total reflection (ATR) infrared spectroscopy provided additional evidence for the assignment based on the anharmonic shift, which is large in the case of Pt-H ($90\,cm^{-1}$) in agreement with the DFT calculations. The absorption cross-section of Pt-H is smaller than that of the very strong Pt-CO vibration by only a modest factor $\sim 1.5 - 3$. Since Pt-H is transiently involved in catalytic water splitting on Pt, the present spectroscopic characterization paves the way for *in-operando* kinetic studies of such reactions.

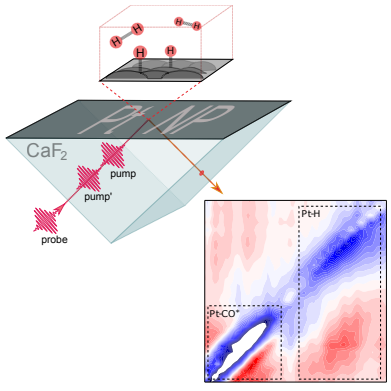

Despite more than 40 years of research, photo/electrocatalytic water splitting still remains elusive from practical large scale application.[1,2] The overall energy conversion efficiency of the water splitting process is low or the catalysts are unstable,[3–5] even though significantly improved performances were manifested for both hydrogen evolution reaction (HER) and oxygen evolution reaction.[6,7] One of the research directions is to employ noble metals as cocatalysts on a large scale of materials such as metal oxides, sulfides, (oxy)nitrides to create active sites and improve the charge separation/recombination properties of catalytic systems.[8] Platinum with its unique position near the top of the volcano plot implies almost ideal affinity to hydrogen and therefore represents a model and benchmarking system for the HER. Besides being the elementary intermediate of the HER, adsorbed hydrogen is also involved as a reaction intermediate in several catalytic hydrogenation reactions of organic compounds on Pt group metals.[9] In this regard, understanding of the Pt-H bond dynamics can have far-reaching consequences for the heterogeneous catalysis in general.

Its structural sensitivity renders infrared (IR) spectroscopy a powerful method to investigate heterogeneous catalytic interfaces. The very first IR study investigating the Pt-H species in the gas phase showed two absorption bands at $2110\,\mathrm{cm}^{-1}$ and $2060\,\mathrm{cm}^{-1}$, which were assigned to weakly (atomically chemisorbed) and strongly bound (interstitially chemisorbed) hydrogen, respectively.[10] Although there is some level of agreement on the assignment of the high energy band to a Pt-H vibration, the low energy band is a subject of controversy. It has been argued in Ref.[11] that the IR transition of interstitially bound hydrogen would be too weak and too broad to be detected by IR spectroscopy due to the absence of a discrete covalent bond to a single Pt atom. Instead, the low energy band has been assigned to linearly bound carbon monoxide formed from carbonate complexes that were present in the alumina support in that particular case. On the other hand, a more recent study, similar to the present work in terms of the sample preparation, reported three IR bands between $1980 - 2080\,\mathrm{cm}^{-1}$, all of which were assigned to Pt-H modes,[12] in contradiction to the works mentioned above. Pt-H has also been studied in water by electrochemically adsorbed hydrogen on various Pt surfaces, identifying overpotential deposited H atoms absorbing around $2080 - 2095\,\mathrm{cm}^{-1}$,[13–15] while weak bands at 2000 and $1800\,\mathrm{cm}^{-1}$ were again assigned to linear and bridged CO, respectively.[14] These obviously conflicting interpretations call for a careful assignment of the IR spectrum. In particular the possibility of adsorbed CO is a challenge in these types of experiments, since organic contamination

can be transformed into CO in the presence of Pt and H_2.[14,16–18] Trace amounts of CO may dominate the IR response in the Pt-H spectral region, since the binding affinity of CO to Pt is much larger than that of H and since the CO stretch vibrational frequency is very close to that of Pt-H but at the same time its absorption cross section is (presumably) larger.

The above mentioned studies[10–17,19–22] employed IR absorption spectroscopy, i.e., linear IR spectroscopy. Nonlinear IR spectroscopy, such as ultrafast IR-pump-IR-probe spectroscopy or 2D IR spectroscopy, may provide significantly enhanced information about structure and dynamics of chemical bonds. With regard to catalytic interfaces, ultrafast 2D attenuated total reflection (ATR) IR spectroscopy has recently been introduced.[23] As it is the case for IR absorption spectroscopy, the ATR geometry has superior surface sensitivity over other measurement configurations.[24] Its combination with 2D IR spectroscopy[25] has been shown to be capable of addressing fundamental questions of adsorbate-adsorbate[26], adsorbate-substrate[27] and adsorbate-solvent[28] interactions.

Here, we report on the ultrafast characterization of the Pt-H bond on the solid/gas interface with the help of ultrafast IR pump-probe spectroscopy in ATR geometry as well as 2D ATR IR spectroscopy, with three main objectives in mind: providing additional criteria for assignment of the Pt-H vibration, distinguishing it from the Pt-CO vibration beyond any doubt and to gain deeper understanding of Pt-H as an elusive intermediate of the HER. In this way, our work paves the way to follow the photo/electrocatalytic hydrogen formation and dynamics *in-situ*.

To set the stage, we compare in Fig. 1a conventional IR absorption spectra of a sample where H_2 and D_2 gases were flown separately over freshly coated Pt surfaces. Upon introducing H_2 to the ATR cell, three distinct bands at $2090\,\mathrm{cm}^{-1}$, $2000\,\mathrm{cm}^{-1}$ and $1800\,\mathrm{cm}^{-1}$ appear. In contrast, D_2 gives rise to only the $2000\,\mathrm{cm}^{-1}$ and $1800\,\mathrm{cm}^{-1}$ bands, indicating that the 2090 cm^{-1} band stems from Pt-H. From a reduced mass argument, the expected isotope shift ratio of $1/\sqrt{2}$ between Pt-H and Pt-D modes anticipates the Pt-D band around $1490\,\mathrm{cm}^{-1}$. However, for both the H_2 and the D_2 experiments, the $1400 - 1500\,\mathrm{cm}^{-1}$ spectral region was congested by several other bands, which did not allow for a clear assignment of the Pt-D band in the data of Fig. 1a (the corresponding spectral region is not shown in Fig. 1a). Most probably, these bands stem from contaminants (carboxylates, carbonates etc.) reduced by H_2 or D_2. It is possible to eliminate these contributions when the reference spectrum is taken while the surface is saturated with H_2 flow for 30 min, and then directly

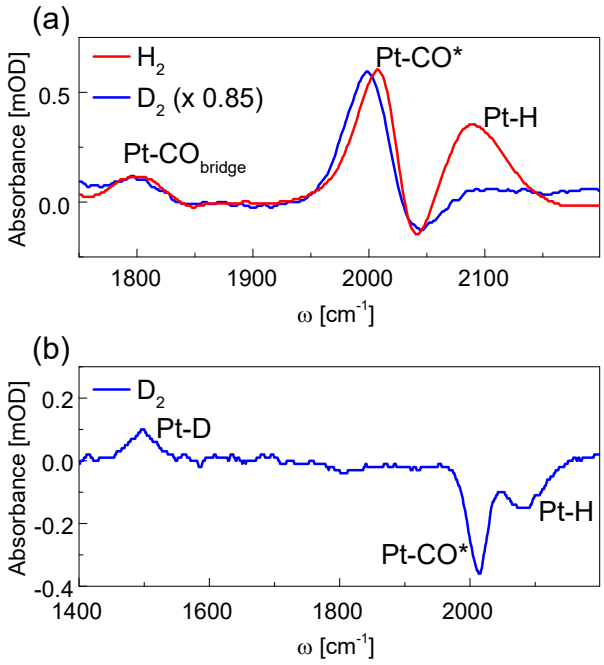

FIG. 1. (a) IR absorption spectra induced by the flow of H_2 (red) and D_2 (blue) gases. (b) Isotope exchange induced by the flow of D_2, when the reference spectrum was taken under H_2 flow.

exchanged to D_2. The obtained isotope exchange difference spectrum shows the disappearance of the 2090 cm^{-1} Pt-H band together with a concomitant appearance of the Pt-D band at 1490 cm^{-1} (Fig. 1b), i.e., the exact position expected from the larger reduced mass of the Pt-D vibration.

The two other bands in Fig. 1a, appearing at 2000 cm^{-1} and 1800 cm^{-1} with both H_2 and D_2, are assigned to CO bound in a linear and bridged configuration to Pt, respectively, in accordance with earlier interpretations.[11,14] The 2000 cm^{-1} band is different from the case when CO gas is adsorbed alone (see Supporting Information, Fig. S1). It is known that hydrogen causes a red-shift of the Pt-CO band when co-adsorbed on Pt, an effect that has been explained by several mechanisms including π-backbonding in metal carbonyls[19], dipole coupling[20,21] and surface restructuring.[22] However, the appearance of such low-frequency Pt-CO band at 2000 cm^{-1} has not been reported before to the best of our knowledge. In order to differentiate the two CO species, the linearly bound CO vibration appearing in the H_2/D_2 experiments will be referred to as "Pt-CO*" throughout the paper. It should be noted that the intensity of the Pt-CO* band varies in different experiments, pointing to the fact that the concentration of CO on the surface vary from sample to sample and also as

a function of time. For example, the Pt-CO* band diminished in intensity in the isotope exchange experiment of Fig. 1b.

The CO contamination can be either present in the source gas (which in the case of H_2 is typically produced by steam reforming) or can be formed by a reaction between H_2 or organic surface contaminants.[14,16,17] Since we employed highest purity gases, gas purifiers for both H_2 and D_2, stainless steel cell and tubings, we tentatively attribute the appearance of the Pt-CO* band to the latter. In addition, Fig. 1a also shows a negative going band at $2040\,\mathrm{cm}^{-1}$ for both the H_2 and the D_2 experiments. Several hours after the H_2 flow is stopped, all the positive features disappear and only the negative $2040\,\mathrm{cm}^{-1}$ remains (see Supporting Information, Fig. S2). This points to the fact that small amount of CO contamination was already present on the Pt surface before starting the experiments, with the $2040\,\mathrm{cm}^{-1}$ band being in the background spectrum. It might very well be that this CO contamination is converted into Pt-CO* upon adsorption of H_2, i.e, an additional source of CO.

Even though the H/D exchange experiment of Fig. 1b strongly supports an assignment of the two bands at $2090\,\mathrm{cm}^{-1}$ and $1490\,\mathrm{cm}^{-1}$ to Pt-H and Pt-D, respectively, the previous confusion in literature[10–17,19–22] leaves enough room for speculations. Therefore, we now turn to nonlinear spectroscopy to provide additional evidence for our assignment. Fig. 2a shows the evolution of IR-pump-IR-probe spectra as a function of the pump-probe delay time under continuous flow of H_2 gas. Two negative going ground state bleach (GSB) and stimulated emission (SE) signals related to the 0-1 transition of the corresponding vibrator are clearly observed. According to the assignment of Fig. 1a, the fast decaying band centered at $2080\,\mathrm{cm}^{-1}$ belongs to Pt-H, while the band around $2000\,\mathrm{cm}^{-1}$ stems from Pt-CO*. The pump-probe signal was averaged within the shaded area in Fig. 2a and fitted to single exponential decay with a lifetime of $(0.8 \pm 0.1)\,\mathrm{ps}$ in Fig. 2b. This is considerably shorter than the lifetime of Pt-CO, which is $2 - 3\,\mathrm{ps}$ in the liquid[29–31] and gas phase[32–34]. As a side-remark we note that the GSB/SE signal from Pt-CO* stays almost constant up to 2 ps (the maximum time range of the experiment in Fig. 2), hence its vibrational lifetime is even longer than what is commonly observed for Pt-CO without co-adsorbed hydrogen. This effect will be investigated further in future work.

Around $1960\,\mathrm{cm}^{-1}$, a positive signal is observed in the pump-probe response (Fig. 2a), which originates from the red-shifted excited state absorption (ESA, 1-2 transition of the

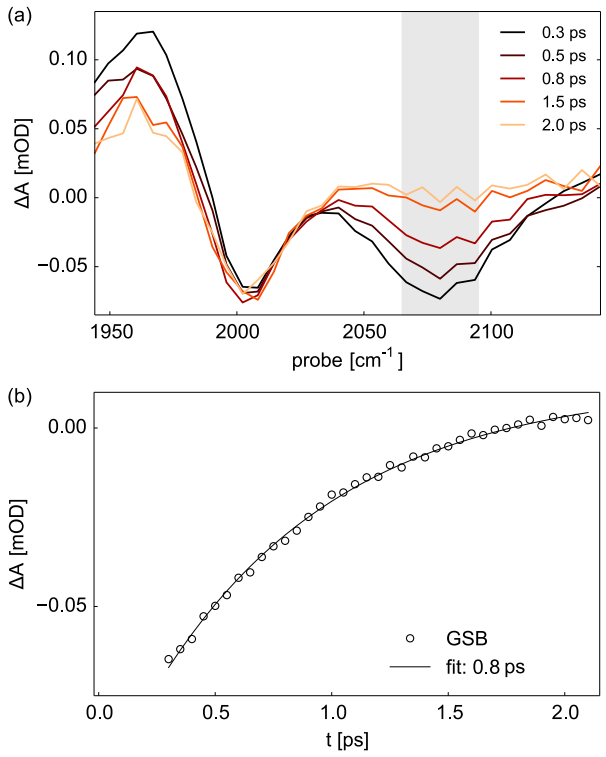

FIG. 2. Pump-probe signals as a function of delay time. (a) The broad and fast decaying GSB and SE signal from Pt-H at 2080 cm^{-1} is accompanied by the more slowly decaying GSB/SE signal centered at 2000 cm^{-1} from Pt-CO*. (b) Single exponential fit to the GSB/SE signal averaged over the shaded area between 2065-2095 cm^{-1} in panel (a).

corresponding vibrator). The band appears to have a quickly decaying component together with one that is essentially constant on the 2 ps time range. We therefore conclude that the ESA signals of both Pt-CO* and Pt-H overlap, but a clear assignment is not possible based on pump-probe spectroscopy.

2D ATR IR spectroscopy, in contrast, can disentangle these overlapping contributions and furthermore, can reveal inter- and intra-band correlations as a result of frequency resolution along the pump axis.[25] Fig. 3 depicts the 2D spectrum at 0.3 ps delay, where the negative GSB/SE (blue) of the Pt-H located on the diagonal illustrates a large inhomogeneous broadening assigned to the structural heterogeneity of the Pt surface. The positive signal appearing at the same pump frequency but red-shifted along the probe axis shows that the ESA (red) maximum of the Pt-H is at 1990 cm^{-1}, which coincides with the Pt-CO* band and it is therefore covered in the pump-probe experiment (Fig. 2a). The anharmonic

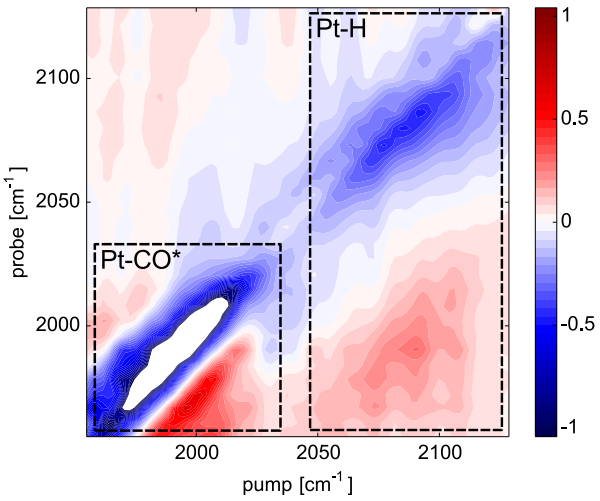

FIG. 3. Normalized 2D ATR IR spectrum of the Pt-H band at a pump-probe delay time of t = 0.3 ps. The inhomogeneously broadened GSB/SE signal of Pt-H (blue) is accompanied by the ESA signal (red) that is anharmonically red-shifted along the probe-frequency axis by $\sim 90\,\mathrm{cm}^{-1}$. The corresponding bands from Pt-CO* reveal a much smaller anharmonic shift of $\sim 20\,\mathrm{cm}^{-1}$.

shift of $\sim 90\,\mathrm{cm}^{-1}$ between the GSB/SE and ESA maxima of the Pt-H vibration is in perfect agreement with results from density functional theory (DFT) calculations for H bound to a slab of Pt ($\sim 92\,\mathrm{cm}^{-1}$, see Figs. S3, S4 and Supporting Information for details). In contrast, Pt-CO* exhibits a significantly lower anharmonic shift of $\sim 20\,\mathrm{cm}^{-1}$ experimentally[30,35], while the DFT calculations predict $\sim 26\,\mathrm{cm}^{-1}$ (see Supporting Information).

Bearing in mind possible future studies of Pt-H intermediates in a transient water-splitting experiment, it is crucially important to estimate the absorption cross section of the Pt-H transition. The absorption cross section of a transition is characterized by its effective transition dipole moment μ^2, which may include both chemical enhancement effects (i.e., change of chemical structure upon binding to the metal) as well as plasmonic enhancement effects due to the nano-structured metal surface.[36] While we do not know the surface area and surface coverage of our sample, which would be needed to determine the transition dipole moment in absolute terms, we can resort to a trick that at least allows us to estimate the effective transition dipole moment relative to that of Pt-CO. The trick builds on the fact that the absorbance S^A scales as μ^2, while the pump-probe signal S^{PP} scales as μ^4.[25]

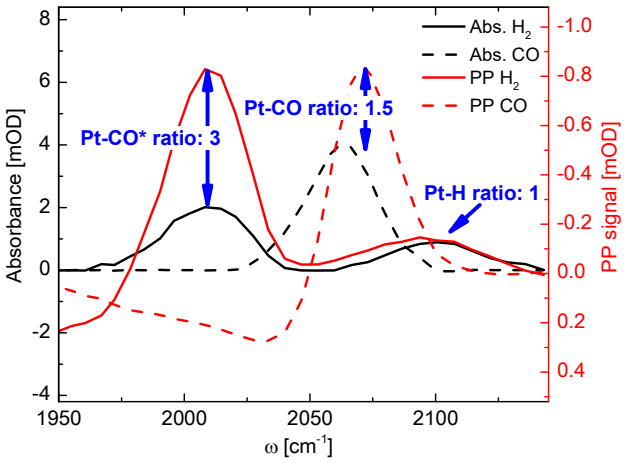

FIG. 4. *In-situ* IR absorption spectra (black, left scale) and pump-probe signals at t=0.3 ps (red, right scale) of Pt-H and Pt-CO* (solid lines) and Pt-CO (dashed lines, the latter being scaled down by a factor 0.3). The right scale for the pump-probe signal is scaled in a way that the IR absorption spectrum of Pt-H is of equal height as its pump-probe signal. The blue arrows indicate the S^{PP}/S^{A} ratios (Eq. 1) of the Pt-CO and the Pt-CO* bands with respect to Pt-H.

When calculating the ratio:[36–38]

$$\frac{S^{PP}_{CO}/S^{A}_{CO}}{S^{PP}_{PtH}/S^{A}_{PtH}} = \frac{n_{CO}\mu^{4}_{CO}/n_{CO}\mu^{2}_{CO}}{n_{PtH}\mu^{4}_{PtH}/n_{PtH}\mu^{2}_{PtH}} = \frac{\mu^{2}_{CO}}{\mu^{2}_{PtH}} \tag{1}$$

the unknown numbers of molecules n_{CO} and n_{PtH} in the probed area cancel out, since they scale linearly for both S^{A} and S^{PP}.

Fig. 4 illustrates the μ^2 ratios extracted from experiment (note that the sample preparation in Fig. 4 has been different from that in Fig. 2, see Materials and Methods for details, and in addition contains a higher contamination with Pt-CO*). For a direct comparison of Pt-CO* *versus* Pt-H, both pump-probe and absorbance spectra had to be measured on exactly the same sample and in the same pump-probe setup. Normalizing the absorbance scale (left scale) to the pump-probe scale (right scale) for the Pt-H bands allows one to read off the ratio given in Eq. 1 for the Pt-CO* band directly. In an independent experiment we also investigated only CO adsorbed to Pt in order to also compare the Pt-CO vibration (Fig. 4, dashed lines, which have been scaled down to match the Pt-CO* pump-probe signal). Considering that CO on metals is a very strong IR absorber,[39] the extracted values of 3 ± 1 (Pt-CO*/Pt-H) and 1.5 ± 0.5 (Pt-CO/Pt-H) for the μ^2 ratios points out to the fact that the transition dipole of Pt-H is sizeable. The corresponding value from the DFT

calculation is ∼2.5 (see Supporting Information for details), in perfect agreement with the experimental result.

In conclusion, we presented a complete characterization of the Pt-H vibrational mode by means of ultrafast nonlinear IR spectroscopy. All measurables deduced from these experiments, which go beyond what could be retrieved from conventional linear absorption spectroscopy, i.e., the vibrational lifetime, anharmonicity and transition dipole, clearly distinguish the Pt-H from the Pt-CO* species. The shorter lifetime of the Pt-H is readily explained by the fact that H is directly coupled to the metallic surface, while the Pt-C bond acts as a spacer for the Pt-CO/CO* modes. The importance of electronic friction for vibrational relaxation of hot hydrogen atoms on metal surfaces has recently been studied with the help of *ab initio* MD simulations,[40] revealing a 0.2 ps cooling time after adsorption of H_2 on Pd(100). Our observation of a somewhat slower time constant (0.8 ps) will serve as a benchmark for the theoretical modelling of electronic friction. The larger anharmonicity of the Pt-H vibration reflects its lower reduced mass, as a result of which it explores a larger region of the potential energy surface. Finally, the sizeable absorption cross section of the Pt-H vibration is a promising result in terms of the detection limit of transiently generated Pt-H in photoelectrocatalysis. The low Pt-H signal despite its large cross section implies that a rather low surface coverage of Pt-H can indeed be detected. Since the Pt-H bond is assumed to play important role in photo/electro catalysis of water and catalytic hydrogenation of organic molecules as a real intermediate, we believe that our results pave the way towards transient measurements to provide in-operando kinetic information for such processes.

Materials and Methods

Stainless steel tubing and a home-built stainless steel sample cell were used in all experiments to prevent any contamination of the gas from the flow system. The tightness of the cell was ensured by a FEP/MVQ O-ring (Kubo Tech AG) pressed in between the stainless steel cell and the ATR surface of the CaF_2 prism. Tubes and cell were purged with Ar (6.0 PanGas AG) prior to H_2/D_2 adsorption in order to eliminate any CO_2 contamination as much as possible. H_2 (6.0 PanGas AG) and D_2 (3.0 PanGas AG) were used together with ambient temperature gas purifiers (MC1-904F, SAES Pure Gas), reducing the gas impurity to less than 1 ppb.

Right angle ATR CaF_2 prisms were coated with an ultra thin Pt layer (99.98 %, Baltic

Präparation) with average thickness of 0.1 nm using a Ar^+-ion sputter coater (Safematic CCU-010 HV) under the following conditions: working distance of 7 cm, current 20 mA, pressure of $8 \cdot 10^{-5}$ mbar and Ar pressure of $5 \cdot 10^{-2}$ mbar, resulting in the sputtering rate of < 0.02 nm/s. With an average Pt thickness of 0.1 nm, the CaF_2 is not homogeneously covered, rather, the Pt forms aggregated patches with lateral extensions between 2 and 10 nm separated by gaps of similar size (see Fig. 1c of Ref.[27]). Such ultra thin metal layers are advantageous for the ultrafast experiments due to their low metal absorption that result in negligible line-shape distortions and reduced scattering.[30,41] Freshly coated prism were used for each experiment in order to ensure the reproducibility of the results. We found that the Pt-H absorption signal was significantly lower when H_2/D_2 was re-adsorbed on an already used prism, for reasons that are currently not clear.

If not noted otherwise, IR absorption spectra were acquired with a commercial Fourier transform (FT)IR spectrometer (Bruker VERTEX 80V) with 4 cm^{-1} spectral resolution. All spectra were corrected for a constant background by zeroing the absorption in a spectral region around 1900 cm^{-1}, accounting for the fact that adsorbed hydrogen changes the electron density in the metal leading to significant background shifts.

The ultrafast 2D ATR IR setup was described in detail elsewhere.[28,42] Briefly, 100 fs short mid-IR pulses centered at 2080 cm^{-1} were generated in an OPA pumped with a 5 kHz amplified Ti-Sapphire laser system (Spectra Physics, Spitfire).[43] The output from the OPA was split into pump, probe and reference beams with a BaF_2 wedge. The pump beam entered a Mach-Zehnder interferometer to create collinear pump pulse pairs for the 2D ATR IR experiments (for the pump-probe experiments, one arm in the interferometer was blocked) with a typical energy of ∼50-120 nJ. All beams were then focused with an off-axis concave mirrors to a CaF_2 prism from the backside with a relative angle of $\sim 15 - 20°$ between pump and probe. Probe and reference beams were spectrally dispersed and imaged with a spectrograph (Jobin-Yvon Triax, 150 lines/mm grating) onto a 2x32 pixel MCT array detector (Infrared Associates) for balanced detection with a resolution of $\sim 6\,cm^{-1}$. To suppress scattering from the nanoparticulate metal layer in the ultrafast measurements, a 4-step quasi phase-cycling scheme was employed with the help of a piezo actuator modulating the probe delay time (1 cycle per 4 pump-probe scans or per ∼ 80 interferograms).[44] The 2D ATR IR spectrum was calculated from ∼ 700 interferograms, each scanned for 3.5 ps along the coherence time (delay between the two pump pulses) and apodized with a cosine

function to reduce noise.

For both FTIR and ultrafast experiments, the angle of incidence with respect to the normal of the reflecting plane of the prism was set relatively close ($\sim 5°$) to the critical angle of the CaF_2/air interface ($\sim 46°$) in order to obtain the maximum signal, yet still far enough to avoid lineshape distortions. We used *s*-polarisation at the prism surface in the ultrafast experiments, since that reveals better defined polarisation conditions and a higher signal enhancement.[36]

Regarding the experiments for determining the transition strength of the Pt-H relative to that of Pt-CO, *in-situ* IR absorption spectra were measured in the ultrafast setup using probe and reference beams. Reference spectra were taken on fresh prisms before introducing any gases to the cell. Several spectra (2000 shots) were averaged. Due to the low signal-to-noise ratio of this configuration, 0.2 nm thick Pt layers were used in this case.

Supporting Information: Additional IR absorption spectra (Figs. S1 and S2) as well as details on the DFT calculations and anharmonic frequency calculations are given in Supporting Information.

Acknowledgments: The authors thank J.P. Kraack for helpful discussions, Roland Zehnder for the help with the design and construction of the gas flow system, and the Center for Microscopy and Image Analysis (University of Zurich) for providing the sputter coating facility. The research was supported by the Swiss National Science Foundation (grant CRSII2_160801/1) and the University Research Priority Program (URPP) for solar light to chemical energy conversion (LightChEC) of the University of Zurich.

---

(1) Maeda, K.; Domen, K. Photocatalytic water splitting: Recent progress and future challenges, *J. Phys. Chem. Lett.* **2010**, *1*, 2655–2661.

(2) Jafari, T.; Moharreri, E.; Amin, A.; Miao, R.; Song, W.; Suib, S. Photocatalytic water splitting–the untamed dream: A review of recent advances, *Molecules* **2016**, *21*, 900.

(3) Mubeen, S.; Lee, J.; Singh, N.; Krämer, S.; Stucky, G. D.; Moskovits, M. An autonomous

photosynthetic device in which all charge carriers derive from surface plasmons, *Nat. Nanotechnol.* **2013**, *8*, 247–251.

(4) Liu, C.; Tang, J.; Chen, H. M.; Liu, B.; Yang, P. A fully integrated nanosystem of semiconductor nanowires for direct solar water splitting, *Nano Lett.* **2013**, *13*, 2989–2992.

(5) Liao, L.; Zhang, Q.; Su, Z.; Zhao, Z.; Wang, Y.; Li, Y.; Lu, X.; Wei, D.; Feng, G.; Yu, Q.; Cai, X.; Zhao, J.; Ren, Z.; Fang, H.; Robles-Hernandez, F.; Baldelli, S.; Bao, J. Efficient solar water-splitting using a nanocrystalline CoO photocatalyst, *Nat. Nanotechnol.* **2014**, *9*, 69–73.

(6) Kalisman, P.; Nakibli, Y.; Amirav, L. Perfect photon-to-hydrogen conversion efficiency, *Nano Lett.* **2016**, *16*, 1776–1781.

(7) Tang, Y.; Wang, R.; Yang, Y.; Yan, D.; Xiang, X. Highly enhanced photoelectrochemical water oxidation efficiency based on triadic quantum dot/layered double hydroxide/$BiVO_4$ photoanodes, *ACS Appl. Mater. Interfaces* **2016**, *8*, 19446–19455.

(8) Maeda, K. Photocatalytic water splitting using semiconductor particles: History and recent developments, *J. Photochem. Photobiol. C* **2011**, *12*, 237–268.

(9) Rylander, P. *Catalytic hydrogenation over platinum metals;* Elsevier, 2012.

(10) Pliskin, W.; Eischens, R. Infrared spectra of hydrogen and deuterium chemisorbed on platinum, *Z. Physik. Chem.* **1960**, *24*, 11–23.

(11) Primet, M.; Basset, J.; Mathieu, M.; Prettre, M. Infrared investigation of hydrogen adsorption on alumina-supported platinum, *J. Catal.* **1973**, *28*, 368–375.

(12) Dong, Y.; Hu, G.; Hu, X.; Xie, G.; Lu, J.; Luo, M. Hydrogen adsorption and oxidation on Pt film : An in situ real-time attenuated total reflection infrared (ATR-IR) spectroscopic study, *J. Phys. Chem. C* **2013**, *117*, 12537–12543.

(13) Nichols, R.; Bewick, A. Spectroscopic identification of the adsorbed intermediate in hydrogen evolution on platinum, *J. Electroanal. Chem.* **1988**, *243*, 445–453.

(14) Kunimatsu, K.; Senzaki, T.; Samjeské, G.; Tsushima, M.; Osawa, M. Hydrogen adsorption and hydrogen evolution reaction on a polycrystalline Pt electrode studied by surface-enhanced infrared absorption spectroscopy, *Electrochim. Acta* **2007**, *52*, 5715–5724.

(15) Ogasawara, H.; Ito, M. Hydrogen adsorption on Pt(100), Pt(110), Pt(111) and Pt(1111) electrode surfaces studied by in situ infrared reflection absorption spectroscopy, *Chem. Phys. Lett.* **1994**, *221*, 213–218.

(16) Dixon, L.-T.; Barth, R.; Gryder, J. Infrared active species of hydrogen adsorbed by alumina-supported platinum, *J. Catal.* **1975**, *37*, 368–375.

(17) Nanbu, N.; Kitamura, F.; Ohsaka, T.; Tokuda, K. Adsorption of atomic hydrogen on a polycrystalline Pt electrode surface studied by FT-IRAS: The influence of adsorbed carbon monoxide on the spectral feature, *J. Electroanal. Chem.* **2000**, *485*, 128–134.

(18) Futamata, M.; Luo, L.; Nishihara, C. ATR–SEIR study of anions and water adsorbed on platinum electrode, *Surf. Sci.* **2005**, *590*, 196–211.

(19) Primet, M.; Basset, J.; Mathieu, M.; Prettre, M. Infrared study of CO adsorbed on $PtAl_2O_3$. A method for determining metal-adsorbate interactions, *J. Catal.* **1973**, *29*, 213–223.

(20) Willis, R.; Lucas, A.; Mahan, G. *Vibrational properties of adsorbed molecules;* Elsevier: Amsterdam, 1983.

(21) Eischens, R. P. Infrared spectra of chemisorbed molecules, *Acc. Chem. Res.* **1972**, *5*, 74–80.

(22) Ferri, D.; Bürgi, T.; Baiker, A. Pt and Pt/Al2O3 thin films for investigation of catalytic solid- liquid interfaces by ATR-IR spectroscopy: CO adsorption, H2-induced reconstruction and surface-enhanced absorption, *J. Phys. Chem. B* **2001**, *105*, 3187–3195.

(23) Kraack, J. P.; Hamm, P. Surface-sensitive and surface-specific ultrafast two-dimensional vibrational spectroscopy, *Chem. Rev.* **2016**, *117*, 10623–10664.

(24) Mojet, B. L.; Ebbesen, S. D.; Lefferts, L. Light at the interface: The potential of attenuated total reflection infrared spectroscopy for understanding heterogeneous catalysis in water, *Chem. Soc. Rev.* **2010**, *39*, 4643–4655.

(25) Hamm, P.; Zanni, M. *Concepts and methods of 2D infrared spectroscopy;* Cambridge University Press: Cambridge, 2011.

(26) Kraack, J. P.; Frei, A.; Alberto, R.; Hamm, P. Ultrafast vibrational energy-transfer in catalytic monolayers at solid-liquid interfaces, *J. Phys. Chem. Lett.* **2017**, *8*, 2489–2495.

(27) Kraack, J. P.; Kaech, A.; Hamm, P. Molecule-specific interactions of diatomic adsorbates at metal-liquid interfaces, *Struct. Dyn.* **2017**, *4*, 044009.

(28) Kraack, J. P.; Lotti, D.; Hamm, P. 2D attenuated total reflectance infrared spectroscopy reveals ultrafast vibrational dynamics of organic monolayers at metal-liquid interfaces, *J. Chem. Phys.* **2015**, *142*, 212413.

(29) Peremans, A.; Tadjeddine, A.; Guyot-Sionnest, P. Vibrational dynamics of CO at the (100) platinum electrochemical interface, *Chem. Phys. Lett.* **1995**, *247*, 243–248.

(30) Lotti, D.; Hamm, P.; Kraack, J. P. Surface-sensitive spectro-electrochemistry using ultrafast 2D ATR IR spectroscopy, *J. Phys. Chem. C* **2016**, *120*, 2883–2892.

(31) Li, J.; Qian, H.; Chen, H.; Zhao, Z.; Yuan, K.; Chen, G.; Miranda, A.; Guo, X.; Chen, Y.; Zheng, N.; Wong, M. S.; Zheng, J. Two distinctive energy migration pathways of monolayer molecules on metal nanoparticle surfaces., *Nat. Commun.* **2016**, *7*, 10749.

(32) Beckerle, J. D.; Casassa, M. P.; Cavanagh, R. R.; Heilweil, E. J.; Stephenson, J. C. Ultrafast infrared response of adsorbates on metal surfaces: Vibrational lifetime of CO/Pt(111), *Phys. Rev. Lett.* **1990**, *64*, 2090–2093.

(33) Backus, E. H. G.; Eichler, A.; Kleyn, A. W.; Bonn, M. Real-time observation of molecular motion on a surface, *Science* **2005**, *310*, 1790–1793.

(34) Arnolds, H.; Bonn, M. Ultrafast surface vibrational dynamics, *Surf. Sci. Rep.* **2010**, *65*, 45–66.

(35) Manceron, L.; Tremblay, B.; Alikhani, M. Vibrational spectra of PtCO and $Pt(CO)_2$ isolated in solid argon: Trends in unsaturated group 10 metal carbonyl molecules, *J. Phys. Chem. A* **2000**, *104*, 3750–3758.

(36) Kraack, J. P.; Kaech, A.; Hamm, P. Surface enhancement in ultrafast 2D ATR IR spectroscopy at the metal-liquid interface, *J. Phys. Chem. C* **2016**, *120*, 3350–3359.

(37) Grechko, M.; Zanni, M. T. Quantification of transition dipole strengths using 1D and 2D spectroscopy for the identification of molecular structures via exciton delocalization: Application to α-helices, *J. Chem. Phys.* **2012**, *137*, 184202.

(38) Donaldson, P. M.; Hamm, P. Gold nanoparticle capping layers: Structure, dynamics, and surface enhancement measured using 2D-IR spectroscopy, *Angew. Chem. Int. Ed.* **2013**, *52*, 634–638.

(39) Vannice, M.; Twu, C. Extinction coefficients and integrated intensities for linear-and bridged-bonded co on platinum, *J. Chem. Phys.* **1981**, *75*, 5944–5948.

(40) Blanco-Rey, M.; Juaristi, J. I.; Díez Muiño, R.; Busnengo, H. F.; Kroes, G. J.; Alducin, M. Electronic friction dominates hydrogen hot-atom relaxation on Pd(100), *Phys. Rev. Lett.* **2014**, *112*, 103203.

(41) Bürgi, T. ATR–IR spectroscopy at the metal–liquid interface: Influence of film properties on anomalous band-shapes, *Phys. Chem. Chem. Phys.* **2001**, *3*, 2124–2130.

(42) Helbing, J.; Hamm, P. Compact implementation of Fourier transform two-dimensional IR

spectroscopy without phase ambiguity, *J. Opt. Soc. Am. B* **2011**, *28*, 171–178.

(43) Hamm, P.; Kaindl, R. a.; Stenger, J. Noise suppression in femtosecond mid-infrared light sources, *Opt. Lett.* **2000**, *25*, 1798–1800.

(44) Bloem, R.; Garrett-Roe, S.; Strzalka, H.; Hamm, P.; Donaldson, P. Enhancing signal detection and completely eliminating scattering using quasi-phase-cycling in 2D IR experiments., *Opt. Express* **2010**, *18*, 27067–27078.